Anisotropy of the upper critical field and its thickness dependence in superconducting FeSe electric-double-layer transistors

Junichi Shiogai,[*] Shojiro Kimura, Satoshi Awaji, Tsutomu Nojima, and Atsushi Tsukazaki

Institute for Materials Research, Tohoku University, Sendai 980-8577, Japan

Anisotropy of superconductivity is one of the fundamental physical parameters for understanding layered iron-based superconductors (IBSs). Here we investigated the anisotropic response of resistive transition as a function of thickness (d) in iron selenide (FeSe) based electric-double-layer transistors (EDLTs) on $SrTiO_3$, which exhibit superconducting transition temperatures T_c as high as 40 K below $d = 10$ nm. According to the analyses of the in-plane ($H_{c2}^{//}$) and out-of-plane ($H_{c2}^{\perp}$) upper critical fields (H_{c2}) and the magnetic field angle dependence of the resistance ($R_s - \theta$) in ultrathin condition, we found that the anisotropy factor $\varepsilon_0 = H_{c2}^{//}/H_{c2}^{\perp}$ is 7.4 in the thin limit of $d \sim 1$ nm, which is larger than that of bulk IBSs. In addition, we observed the shorter out-of-plane coherence length ξ_c of 0.19 nm compared to the c-axis lattice constant, which implies the confinement of the order parameter in the one unit cell FeSe. These findings suggest that high-T_c superconductivity in the ultrathin FeSe-EDLT exhibits an anisotropic three-dimensional (3D) or quasi-two-dimensional (2D) nature rather than the pure 2D one, leading to the robust superconductivity. Moreover, we carried out the systematic evaluation of the anisotropic H_{c2} against thickness reduction in the FeSe channel. The in-plane H_{c2} as a function of normalized temperature T/T_c is almost independent of d until the thin limit condition. On the other hand, the out-of-plane H_{c2} near $T/T_c \sim 1$ decreases with increasing d, resulting in the increase of ε_0 at around T_c to 32.0 at the thick condition of $d = 9.3$ nm, which is also confirmed by $R_s - \theta$ measurements. The counterintuitive behavior can be attributed to the degree of coupling strength between two electron-rich layers possessing a high superconducting order parameter induced by electrostatic gating at the top interface and charge transfer from $SrTiO_3$ substrates at the bottom interface. Besides a large $H_{c2}^{\perp}$ for $d = 9.3$ nm exceeding 20 T even at $T = 0.8T_c$, we observe the decoupling crossover of the two superconducting layers at low temperature, which is a unique feature for the high-T_c FeSe-EDLT on $SrTiO_3$.

I. INTRODUCTION

Superconducting anisotropy in layered materials [1–12] and artificial superlattice or heterostructure [13–16] is one of the most important issues not only for actual applications such as superconducting wires [17] but also in-depth understanding of the pairing mechanisms. The class of iron-based superconductors (IBSs) [18–21] commonly possesses stacking of Fe square lattice sheets along the crystallographic c-axis direction. From the crystallographic analogy to the cuprate superconductors, the quasi-two-dimensional Fermi surface of IBSs may be closely linked to the high transition temperature (T_c) superconductivity. Nevertheless, unlike strongly anisotropic superconductivity in cuprates [3–6], the bulk single crystals of IBSs exhibit nearly isotropic upper critical field (H_{c2}). For instance, the zero-temperature anisotropy factor $\varepsilon(T = 0) = H_{c2}^{//\langle 001 \rangle}/H_{c2}^{\perp \langle 001 \rangle}$ approaches unity in 122-type $(Ba,K)Fe_2As_2$ [8] and $\varepsilon(T = 0) \sim 1.2$ or 1.8 in 11-type FeSe [9,22].

The recently discovered high-T_c superconductivity in monolayer FeSe film on $SrTiO_3$ substrate has received growing interest for enhanced critical parameters such as T_c, critical current density, and critical magnetic field [23,24]. The gap closing temperature around 65 K and the resistive transition

temperature around 40 K have been reported [23], both of which are much higher than the bulk $T_c \sim 8$ K [21]. Actually, the electrical transport measurement in high magnetic field $\mu_0 H$ has revealed that the transition is strongly anisotropic with the very large in-plane $\mu_0 H_{c2} > 50$ T at $T = 10$ K [24]. Among such high-T_c thin film studies, the FeSe electric-double-layer transistors (EDLTs) are a useful system because of the controllability of the doping degree and thickness in a single device, which can exclude the sample-to-sample variation of the qualities of the film itself or/and interface between film and substrate [25,26]. Although the evolution of high-T_c superconductivity as a function of charge accumulation and thickness reduction in the FeSe-EDLTs has been reported in our previous studies [25,26], the anisotropy of superconductivity in the monolayer FeSe based on $\mu_0 H_{c2}$ measurements and its variation with thickness have not been clearly addressed so far. This would lead to deeper understanding of its high-T_c superconductivity in FeSe. In the FeSe-EDLT on $SrTiO_3$ substrate, especially, there are two electron-rich layers at the top and bottom interfaces, which are coupled through the middle bulky region with lower T_c than that at the interfaces [26], indicating a nonmonotonic distribution of local superconducting order parameter $\Delta_{SC}(z)$ along thickness direction z. Such a local variation of $\Delta_{SC}(z)$ along the film thickness, distinct from bulk FeSe, would lead to a peculiar anisotropic response of superconducting transitions against magnetic field $\mu_0 H$.

---

[*]junichi.shiogai@imr.tohoku.ac.jp

In this study, we focus on the anisotropy of $\mu_0 H_{c2}$ in FeSe-EDLTs by measuring sheet resistance R_s as functions of temperature, magnetic field, its direction, and film thickness. Here, the film thickness was varied by electrochemical etching in the EDLT configuration [25]. We show that the high-T_c superconductivity in FeSe-EDLTs with the thickness below 10 nm exhibits a larger anisotropy factor than that in low-T_c bulk FeSe. Especially, when the thickness is reduced down to a monolayer, we extract the out-of-plane coherence length $\xi_c \sim 0.19$ nm, which is much shorter than the c-axis lattice spacing of 0.55 nm. This indicates the complete confinement of the Cooper pairs in each FeSe monolayer at low temperature, resulting in the extremely anisotropic 3D (quasi-2D) superconductivity. We also find the unexpected increase in the anisotropy factor near T_c with increasing thickness and the peculiar upturn behavior of out-of-plane H_{c2} as a function of sample temperature in thick $d \sim 9.3$ and 6.3 nm condition. We conclude that such unique characters in FeSe-EDLT stem from the degree of coupling strength between the top and bottom superconducting layers, which becomes strong with decreasing thickness.

II. EXPERIMENTAL DETAILS

The FeSe-EDLT samples were fabricated from two FeSe films grown on nondoped SrTiO₃ (001) insulating substrates with the initial thickness of 15.0 nm (sample A) and 14.8 nm (sample B) by pulsed laser deposition. Schematics of sample geometry and measurement configuration are shown in the top panel in Fig. 1(a). The indium pads were attached onto the FeSe film surface to form Ohmic contacts. A platinum plate was used as a gate electrode. The detailed conditions for film growth and device fabrication are also described in Ref. [25]. The sheet resistance R_s was measured by the dc four-probe

method using an excitation current of 1 μA applied along the $\langle 100 \rangle$ crystallographic axis of FeSe. For the electrostatic EDLT operation, the gate voltage $V_G = 5$ V was applied at sample temperature $T = 220$ K, causing the electron accumulation at the FeSe surface within d_{EDL} [26] as shown in the bottom panel in Fig. 1(a). In addition to the d_{EDL}, the charge transfer from SrTiO₃ substrate forms an electron-rich layer within d_{CT} at the bottom interface [26]. To vary the thickness of FeSe, the sample temperature was increased above 240 K at $V_G = 5$ V, leading to the quasi layer-by-layer electrochemical etching. Thickness of the FeSe films after the sequential etching was estimated under the assumption that the etching rate was proportional to temporal integration of the gate leak current consumed during the etching [25]. The detailed etching scheme and thickness estimation are described in Ref. [25].

The angle dependence measurements in sample A were carried out using a rotatable sample probe loaded into a Physical Property Measurement System equipped with a 9-T superconducting magnet (Quantum Design Co.). The external magnetic field $\mu_0 H$ was applied along the direction with the angle θ from the normal of the film plane. As illustrated in Fig. 1(a), $\theta = 0°$ corresponds to the field direction applied perpendicular to the film plane ($\mu_0 H_\perp$) and $\theta = 90°$ to that parallel to the current ($\mu_0 H_{//}$). For the measurements of angular dependence, θ was scanned from 0° to 120° by rotating the sample stage under the constant magnetic field at 3, 6, and 9 T. The high-field measurements in sample B were performed using a 25-T cryogen-free superconducting magnet system at High Field Laboratory for Superconducting Materials at Institute for Materials Research, Tohoku University [27,28].

III. RESULTS AND DISCUSSION

A. Thickness dependence of the superconducting transition temperature

Figure 1(b) shows T dependence of the normalized sheet resistance $R_s(T)/R_s(100 \text{ K})$ at zero magnetic field for sample A at different thickness under $V_G = 5$ V. When d was decreased below the critical thickness of $d \sim 10$ nm by electrochemical etching, the insulating behavior at the initial thick condition converted a clear superconducting behavior with zero resistance, which is consistent with our previous study [25]. The inset of Fig. 1(b) shows the onset T_c (T_c^{on} is defined as a black arrow in the main panel) as a function of d. As illustrated in bottom panel of Fig. 1(a), FeSe-EDLT under the positive V_G is composed of two electron-rich layers at the top (denoted with the effective thickness d_{EDL}) and at the bottom (denoted with d_{CT}) and the bulky semimetallic middle layer in between them. The electron accumulation within each d_{EDL} and d_{CT} occurs due to electrostatic charge doping at the IL/FeSe interface and due to the charge transfer at the FeSe/SrTiO₃ interface, respectively. Such electron accumulation is closely linked to the emergence of the high-T_c superconductivity [26,29,30]. When the middle layer becomes thin enough to the extent that the local superconducting order parameters of the two electron-rich layers are coupled through the proximity effect, the whole film becomes superconducting with zero resistance. This scenario for emerging high-T_c superconductivity has been discussed with regards to the thickness dependence of Hall coefficient measurements in our previous work [26].
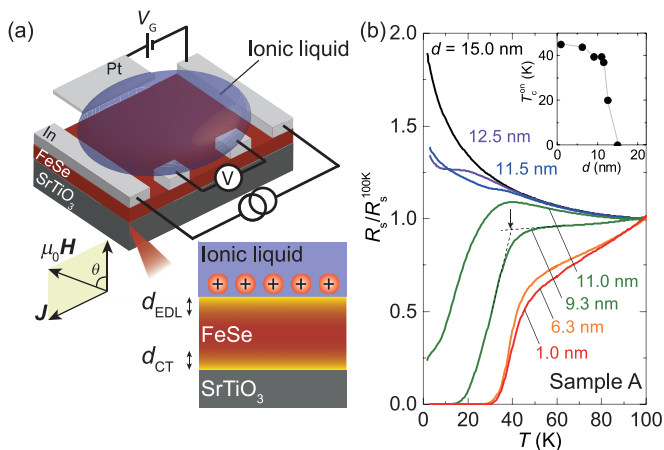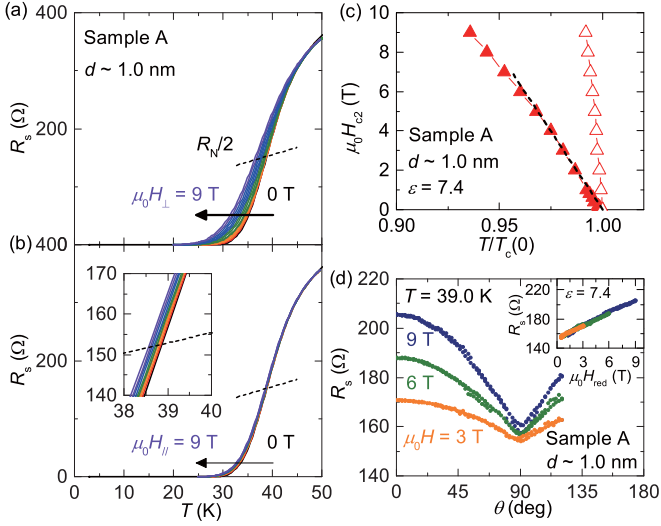

FIG. 1. (a) Schematics of measurement configuration in FeSe-EDLT device (not to scale, left top) and cross section of electron accumulation (right bottom) from top ionic gating within d_{EDL} and bottom charge transfer within d_{CT}. (b) Sheet resistance R_s as a function of temperature T at zero magnetic field under $V_G = 5$ V. For clarity, R_s is normalized to the value at $T = 100$ K. The thickness d was tuned by a series of electrochemical events. Inset: Thickness dependence of onset T_c (T_c^{on}: the intersection of extrapolation lines from normal state and superconducting transition).

FIG. 2. (a), (b) Sheet resistance R_s as a function of temperature T at $V_G = 5$ V for the film thickness $d \sim 1$ nm under the (a) out-of-plane ($\mu_0 H_\perp$) and (b) in-plane ($\mu_0 H_{//}$) magnetic field, respectively. The field increases in steps of 0.2 T from zero (black solid line) to 1 T and in steps of 1 T from 2 to 9 T (purple solid line). Dashed lines are extrapolation of half resistance curves, $0.5 R_s(T)$, in the normal state which define midpoint superconducting transition temperatures $T_c(H)$. Insets: Enlarged views of $R_s(T)$ in the transition region near T_c. (c) In-plane (open symbols) and out-of-plane (filled symbols) upper critical field $\mu_0 H_{c2}$ of FeSe-EDLT (sample A) for $d \sim 1.0$ nm. Out-of-plane $\mu_0 H_{c2} - T_c$ plots follow a linear relation around $T_c(0)$ (black dashed lines). (d) R_s as a function of the angle of applied magnetic field at $T = T_c(0) = 39.0$ K under $\mu_0 H = 3$ (orange), 6 (green), and 9 T (blue) in sample A for $d \sim 1.0$ nm. Inset shows the same trace of $R_s(\theta)$ as a function of reduced magnetic field $\mu_0 H_{red}$ (see text).

B. Anisotropic H_{c2} in monolayer-thick condition

First, we focus on the nearly monolayer-thick condition with $d \sim 1.0$ nm under the gate voltage $V_G = 5$ V in terms of the anisotropy in the upper critical field. Figures 2(a) and 2(b) show $R_s - T$ curves in sample A around the superconducting transition at $d \sim 1$ nm under the out-of-plane ($\mu_0 H_\perp$) and in-plane ($\mu_0 H_{//}$) field from 0 to 9 T. The application of $\mu_0 H_\perp$ slightly broadens the superconducting transition at about 5 K within the experimental range of 9 T. On the other hand, the $\mu_0 H_{//}$ makes a much smaller change in the resistive transition, which is less than 1 K as shown in the insets in Fig. 2(b). The superconducting transition, surviving with a minor change in R_s even in the magnetic field up to 9 T both along the in-plane and out-of-plane directions, indicates the robust high-T_c state in FeSe in the thin limit. Nevertheless, the dramatic difference in the broadening behavior of $R_s(T)$ against magnetic field direction evidences that the high-T_c state of the ion-gated FeSe possesses a highly anisotropic nature.

For a quantitative analysis of the anisotropy in FeSe-EDLT at $d \sim 1.0$ nm, we plot the contours of the in-plane and out-of-plane upper critical fields, $\mu_0 H_{c2}^{//}$ and $\mu_0 H_{c2}^\perp$, in the $\mu_0 H$ versus T plane in Fig. 2(c). We determined $T_c(H)$ that corresponds to the temperature on $H_{c2}(T)$ line by the crossing temperature of the $R_s - T$ transition curves and half of normal state resistance as shown in the dashed lines in Figs. 2(a) and 2(b) [4]. Closed

and open symbols in Fig. 2(c) represent $\mu_0 H_{c2}^\perp$ and $\mu_0 H_{c2}^{//}$. The highly anisotropic behavior with $H_{c2}^{//}(T) \gg H_{c2}^\perp(T)$ is observed, in which $\mu_0 H_{c2}^{//}(T)$ sharply rises with almost linear temperature dependence up to 9 T. We first analyzed the $H_{c2}(T)$ data close to $T_c(0)$ by employing a 3D Ginzburg-Landau (GL) model, described as

$$H_{c2}^\perp(T) = H_{c2}^\perp(0)\left[1 - \frac{T}{T_c(0)}\right], \quad (1)$$

and

$$H_{c2}^{//}(T) = H_{c2}^{//}(0)\left[1 - \frac{T}{T_c(0)}\right], \quad (2)$$

with $\mu_0 H_{c2}^\perp(0)$ and $\mu_0 H_{c2}^{//}(0)$ being the out-of-plane and in-plane upper critical field linearly extrapolated from $H_{c2}(T)$ around $T = T_c(0)$ to zero temperature limit, respectively. The results for the out-of-plane direction are presented in the black dashed lines in Fig. 2(c). The obtained values of $\mu_0 H_{c2}^\perp(0)$ and $\mu_0 H_{c2}^{//}(0)$ are 159 and 1183 T for $d \sim 1.0$ nm, respectively. Note that the analysis by the 2D GL model provided unrealistic parameters where the extracted effective superconducting thickness was much larger than the sample thickness d. The corresponding anisotropy factor determined by the ratio $H_{c2}^{//}/H_{c2}^\perp$ around $T \sim T_c(0)$, $\varepsilon_0(T_c)$, obtained from the 3D GL model, was 7.4. This value is larger than that for the low-T_c bulk FeSe ranging from $\varepsilon(0) = 1.8$ to $\varepsilon(T_c) = 5.2$ [22].

The anisotropy factor $\varepsilon_0(T_c)$ was evaluated by different experiments. Figure 2(d) presents angular θ dependence of the sheet resistance $R_s(\theta)$ at a fixed temperature of $T_c(0)$ under $\mu_0 H = 3$ (blue), 6 (green), and 9 T (orange) for sample A with $d \sim 1.0$ nm. The $R_s(\theta)$ exhibits a round dip (not cusplike) structure around $\theta = 90°$, which was again consistent with the anisotropic 3D nature. Along with the 3D GL effective mass model, it is inferred that $R_s(\theta)$ at various $\mu_0 H$ can be scaled by the reduced magnetic field,

$$H_{red}(\theta) = H\sqrt{\cos^2\theta + \varepsilon^{-2}\sin^2\theta}, \quad (3)$$

where $\varepsilon = \sqrt{m_c/m_{ab}} = H_{c2}^{//}/H_{c2}^\perp$ with m_c and m_{ab} the effective mass perpendicular and parallel to the film plane. When an appropriate ε is given, $R_s(\theta)$ can be scaled by $H_{red}(\theta)$ as exemplified in cuprate superconductor films [31,32] and YBa$_2$Cu$_3$O$_y$/PrBa$_2$Cu$_3$O$_y$ superlattices [33]. The inset in Fig. 2(d) shows the replots of the data of $R_s(\theta)$ in the main panel of Fig. 2(d) against $\mu_0 H_{red}$ with substitution of the same $\varepsilon_0(T_c)$ obtained from Fig. 2(c) for ε in Eq. (3). All three data sets taken under different magnetic fields of $\mu_0 H = 3$, 6, and 9 T superimpose onto a single curve with a fixed $\varepsilon_0(T_c) = H_{c2}^{//}/H_{c2}^\perp$. This result is consistent with the 3D GL effective mass model. Based on these analyses and the $H_{c2}(T)$ plot, which have not been clearly addressed so far in the monolayer high-T_c FeSe, we can conclude that the FeSe-EDLT at $d \sim 1$ nm exhibits an anisotropic 3D superconductivity (quasi-2D). Actually, along the 3D GL model, we can estimate the in-plane and out-of-plane coherence length, $\xi_{ab}(0)$ and $\xi_c(0)$, using the relations $\mu_0 H_{c2}^\perp(0) = \frac{\Phi_0}{2\pi \xi_{ab}^2(0)}$ and $\mu_0 H_{c2}^{//}(0) = \frac{\Phi_0}{2\pi \xi_{ab}(0)\xi_c(0)}$. The extracted values of $\xi_{ab}(0)$ and
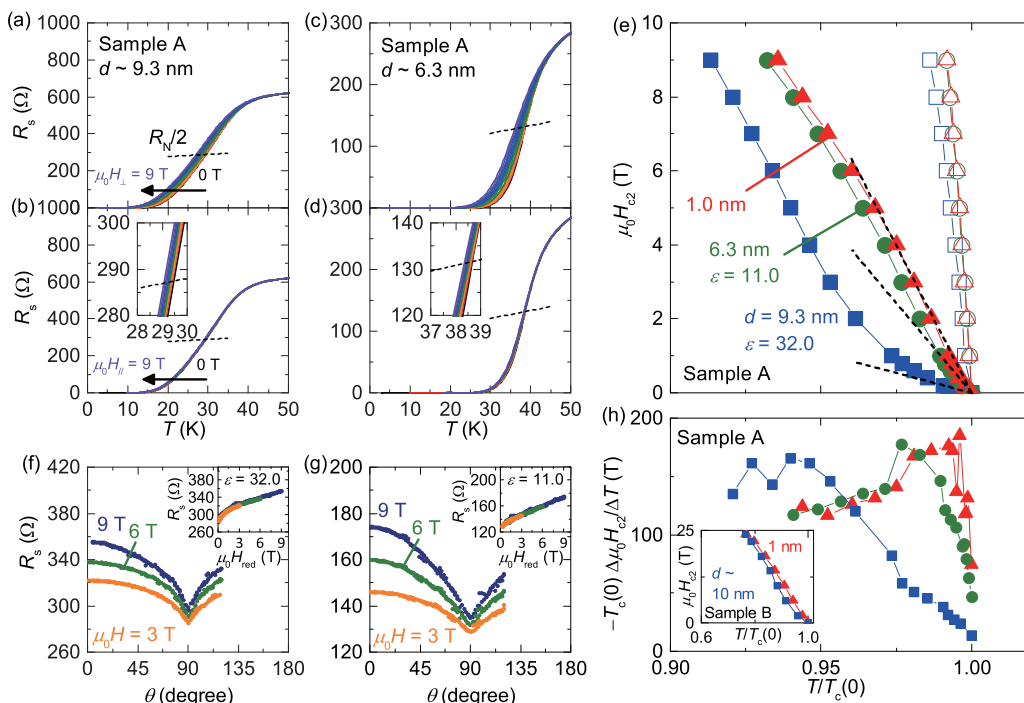
FIG. 3. (a), (b) Sheet resistance R_s as a function of temperature T at $V_G = 5$ V for the film thickness $d \sim 9.3$ nm under the (a) out-of-plane $\mu_0 H_\perp$ and (b) in-plane $\mu_0 H_{//}$ magnetic field, respectively. Insets: Enlarged views of $R_s(T)$ in the transition region near T_c. (c), (d) The same traces of (a), (b) for $d \sim 6.3$ nm. (e) In-plane (open symbols) and out-of-plane (filled symbols) upper critical field H_{c2} of FeSe-EDLT (sample A) for $d \sim 9.3$ (blue squares), 6.3 (green circles), and 1.0 nm [red triangles, the same data from Fig. 2(c)]. Out-of-plane $H_{c2}-T_c$ plots follow a linear relation around $T_c(0)$ (black dashed lines). (f), (g) R_s as a function of the angle of applied magnetic field at $T = T_c(0)$ under $\mu_0 H = 3$ (orange), 6 (green), and 9 T (blue) in sample A for (f) $d = 9.3$ [$T_c(0) = 29.3$ K] and (g) $d = 6.3$ nm [$T_c(0) = 38.9$ K]. Inset shows the same trace of $R_s(\theta)$ as a function of reduced magnetic field $\mu_0 H_{red}$ (see text). (h) The slope of the $\mu_0 H_{c2}^\perp - T_c$ plot in (e) defined as $-T_c(0) \Delta \mu_0 H_{c2}^\perp / \Delta T$. Inset: $\mu_0 H_{c2}^\perp - T_c$ plots of FeSe-EDLT (sample B) for $d \sim 10$ nm (blue filled squares) and 1.0 nm (red filled triangles) measured up to 24 T.

$\xi_c(0)$ are 1.4 and 0.19 nm for FeSe-EDLT at $d \sim 1.0$ nm. The value of $\xi_c(0)$ being smaller than the c-axis lattice constant ~ 0.55 nm means that the order parameter is confined within the one-monolayer thickness at low temperature, leading to the robust 3D superconductivity.

As reported in angle-resolved photoemission spectroscopy (ARPES) [34], the electron-doped monolayer of FeSe with high T_c shows the nearly isotropic Fermi surface with almost degenerate d_{xz}/d_{xy}, d_{yz}, and d_{xy} orbitals around the M point and the disappearance of the hole pocket mainly constituted by the $d_{yz}(d_{xz})$ orbital at the Γ point. Thus, we speculate that the relative increase in the population of the d_{xy} orbital might be linked to the increase in anisotropy of FeSe-EDLT in the thin limit.

C. Anisotropic H_{c2} in multilayer-thick condition

Next, we discuss the anisotropic H_{c2} in the multilayer FeSe. Figures 3(a)–3(d) show $R_s - T$ curves in sample A at relatively thick conditions under $\mu_0 H_\perp$ and $\mu_0 H_{//}$ from 0 to 9 T [(a), (b) for $d \sim 9.3$ nm and (c), (d) for 6.3 nm], respectively. Similarly with the case of $d \sim 1.0$ nm presented in Figs. 2(a) and 2(b), the response of superconducting transition against $\mu_0 H_\perp$ and $\mu_0 H_{//}$ is strongly anisotropic in the relatively thick condition.

The contour plots of $\mu_0 H_{c2}^{//}$ and $\mu_0 H_{c2}^\perp$ in the $\mu_0 H$ versus T plane are presented in Fig. 3(e). The blue, green, and red symbols represent data for $d \sim 9.3, 6.3$, and 1.0 nm [the same trace with Fig. 2(c)], respectively. For all the thickness

conditions, we observe the highly anisotropic H_{c2} with a linear and sharper rise in $\mu_0 H_{c2}^{//}(T)$ with decreasing T. In addition, the variation of $\mu_0 H_{c2}^{//}(T)$ with d is much smaller as compared with the relation of $\mu_0 H_{c2}^{//} \propto 1/d$ expected from the 2D Ginzburg-Landau (GL) theory. This implies that all the thickness conditions in FeSe-EDLT have an anisotropic three-dimensional (3D) or quasi-two-dimensional (2D) nature rather than the pure 2D one. In contrast, for the out-of-plane measurements, we obtained a clear thickness dependence in $\mu_0 H_{c2}^\perp(T)$. The slope of the $\mu_0 H_{c2}^\perp(T)$ around $T_c(0)$ strongly depends on thickness and temperature. This indicates that the average in-plane coherence length, which determines $\mu_0 H_{c2}^\perp$, is dramatically modified by d reduction near $T_c(0)$. The $H_{c2}(T)$ data at around $T_c(0)$ are fitted using Eqs. (1) and (2) as presented in the black dashed lines in Fig. 3(e). The obtained values of $\mu_0 H_{c2}^\perp(0)$ and $\mu_0 H_{c2}^{//}(0)$ are 21.4 and 684 T for $d \sim 9.3$ nm, and 96.6 and 1063 T for $d \sim 6.3$ nm, respectively. The corresponding anisotropy factor $\varepsilon_0(T_c) = H_{c2}^{//}/H_{c2}^\perp$ around $T \sim T_c(0)$ was 32.0 and 11.0, respectively, both of which are larger than that for FeSe-EDLT at $d \sim 1.0$ mm. The fact that the obtained anisotropy factors in FeSe-EDLT become smaller with thickness reduction is contrary to intuitive understanding of superconductivity in reduced dimension. The origin of the decrease of $\varepsilon_0(T_c)$ with decreasing d will be discussed later in relation to Fig. 4.

In order to check the consistency for the counterintuitive d dependence of anisotropy, we examined the scaling behavior of
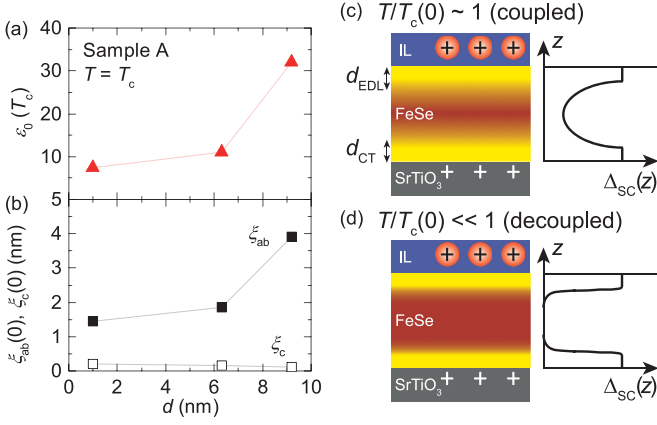
FIG. 4. (a), (b) Thickness dependence of (a) $\varepsilon_0(T_c)$ and (b) $\xi_{ab}(0)$ (filled squares) and $\xi_c(0)$ (open squares) in FeSe-EDLT (sample A). (c), (d) Schematic of distribution of superconducting order parameter $\Delta_{SC}(z)$ for (c) coupled state and (d) decoupled state of FeSe-EDLT for the thick condition (not to scale).

$R_s(\theta)$ for the thick conditions in a similar manner as in Fig. 2(d). Figures 3(f) and 3(g) present $R_s(\theta)$ at $T_c(0)$ under $\mu_0 H = 3$ (blue), 6 (green), and 9 T (orange) for $d \sim 9.3$ and 6.3 nm, respectively. For all the thicknesses, $R_s(\theta)$ exhibits the similar round dip structure around $\theta = 90°$ with the case of $d \sim 1.0$ nm, which was again consistent with the anisotropic 3D nature as presented in the $\mu_0 H_{c2}^{//}(T)$ almost independent of d. Then $R_s(\theta)$ curves $d = 9.3$ and 6.3 nm are replotted against H_{red} in Eq. (3) using the $\varepsilon_0(T_c) = H_{c2}^{//}/H_{c2}^{\perp}$ determined from Fig. 3(e) for ε. As shown in the insets of Figs. 3(f) and 3(g) for both thicknesses, the data points under different $\mu_0 H$ superimpose onto a single curve, meaning the validity of $\varepsilon_0(T_c)$ derived from $H_{c2}^{//}/H_{c2}^{\perp}$ in Fig. 3(e), which decreases with decreasing d.

When looking to the low-$T/T_c(0)$ and high-$\mu_0 H_\perp$ region of Fig. 3(e), we note the peculiar upturn behavior of $H_{c2}^{\perp}(T)$ for thicker samples ($d \sim 9.3$ and 6.3 nm), which is distinct from bulk FeSe and less pronounced for the monolayer-thick one ($d \sim 1.0$ nm). Due to the upturn, the slope of $\mu_0 H_{c2}^{\perp}(T)$ curves for three different d, showing the strong d dependence around $T_c(0)$, seems to approach a similar value. This can be more visible in the local derivative of $H_{c2}^{\perp}(T)$, $-T_c(0)(\Delta\mu_0 H_{c2}/\Delta T)$, as shown in Fig. 3(h). Around $T_c(0)$, the value of $-T_c(0)(\Delta\mu_0 H_{c2}/\Delta T)$ is larger when d becomes smaller. With decreasing $T/T_c(0)$, these values for three different d approach a similar value below $0.95 T_c(0)$. As a consequence, the coherence length at around $T_c(0)$ depends on FeSe thickness, but that at low temperature converges to a similar value.

The upturn and merging behavior in $\mu_0 H_{c2}^{\perp}(T)$ was reexamined by comparing the data for $d \sim 10$ nm and 1.0 nm in the other FeSe-EDLT (sample B) under the higher magnetic field up to 24 T as shown in the inset of Fig. 3(h). The superconductivity with zero resistance survives even at 24 T with the systematic decrease in $T_c(H)$, only by 24% for the out-of-plane condition. Similarly to the case of sample A, the $\mu_0 H_{c2}^{\perp}(T)$ for the thick condition $d \sim 10$ nm exhibits upturn behavior while that for the ultrathin condition $d \sim 1$ nm shows an almost linear

dependence. Following this upturn, we also observe that the $\mu_0 H_{c2}^{\perp}(T)$ line for $d \sim 10$ nm merges to the line for $d \sim 1.0$ nm in low-temperature region of $T \sim 0.8 T_c(0)$.

D. Thickness dependence of anisotropic factor

Figures 4(a) and 4(b) summarize the thickness dependence of the anisotropy factor $\varepsilon_0(T_c)$ and in-plane and out-of-plane coherence length $\xi_{ab}(0)$ and $\xi_c(0)$ for sample A, where $\varepsilon_0(T_c)$ and $\xi_{ab}(0)$ show a positive correlation. The value of $\xi_{ab}(0)$ becomes smaller with reducing d from 3.9 nm ($d \sim 9.3$ nm) to 1.4 nm ($d \sim 1.0$ nm), while that of $\xi_c(0)$ exhibits little dependence on d with 0.14–0.19 nm. Therefore, the difference in $\xi_{ab}(0)$ causes the increase in $\varepsilon_0(T_c)$ with d. The previous study in FeSe-EDLT on SrTiO$_3$ has revealed that the high-T_c superconductivity in FeSe-EDLT appears when the top and bottom electron accumulation layers couple through the middle bulk region at $T_c(0)$ [26]. Thus, we speculate the change of $\xi_{ab}(0)$ and $\varepsilon_0(T_c)$ with d is driven by the weak superconductivity in the middle bulky layer, resulting from the nonmonotonic spatial variation of superconducting order parameter $\Delta_{SC}(z)$ in the FeSe channel. As reported in the previous study, the effective thicknesses of two electron accumulation layers, d_{EDL} and d_{CT}, were estimated to be about 3 and 4 nm, respectively [26], meaning that below $d = 7$ nm a rather uniform super-conducting channel is formed in the FeSe-EDLT driven by strong coupling between these layers. When $\Delta_{SC}(z)$ is weakly coupled along the z direction in the thick FeSe condition near zero magnetic field and $T_c(0)$ as shown in the schematic in Fig. 4(c), the weak Δ_{SC} at the hole-rich bulky layer can work to enlarge the average in-plane coherence length ξ_{ab}. This leads to the decrease in the slope in $\mu_0 H_{c2}^{\perp}(T)$ around $T_c(0)$ [the black dashed lines in Fig. 3(e)] and so the increase in $\varepsilon_0(T_c)$ for thicker condition. At low T under the large $\mu_0 H_\perp$, on the other hand, both of ξ_{ab} and ξ_c at the top and bottom layers shrink, leading to the reduction of the coupling between them as shown in Fig. 4(d). Here, we note that d_{EDL} and d_{CT} can take different values. In this situation, the experimentally evaluated ξ_{ab} is governed solely by these two layers with the strong Δ_{SC}, which behave as decoupled superconducting planes. The emergence of decoupled layers, which results in similar superconducting properties as that for the monolayer FeSe sheet, can explain the coincidence of the slope of $H_{c2}^{\perp}(T)$ for the thick condition with that for the monolayer condition ($d \sim 1.0$ nm) at low T. Thus, the upturn in $H_{c2}^{\perp}(T)$ for the thick condition observed at low T can be the crossover phenomenon from the coupled state in Fig. 4(c) to the decoupled state in Fig. 4(d) between the top and bottom layers.

IV. CONCLUSIONS

We have performed an investigation of anisotropy of the upper critical field $\mu_0 H_{c2}$ in the FeSe-EDLT on SrTiO$_3$ substrate through transport measurements. For the whole FeSe thickness, robust superconductivity with high T_c and significant anisotropy in FeSe has been firmly detected. We determine the $H_{c2} - T$ phase diagram, the in-plane and out-of-plane coherence lengths, and the anisotropy factor, none of which has been explicitly discussed so far. The large but finite anisotropy factor $\varepsilon_0(T_c)$ with an out-of-plane coherence length shorter than the

interlayer spacing of FeSe indicates that the FeSe-EDLT has an anisotropic three-dimensional (3D) or quasi-two dimensional (2D) nature rather than the pure 2D one even in the thin limit, which may be an origin of the robust superconductivity in the monolayer FeSe. In addition, we found that the out-of-plane H_{c2} strongly depends on thickness while the in-plane H_{c2} shows little thickness dependence. Especially, the out-of-plane $H_{c2}(T)$ exhibits anomalous upturn behavior with decreasing T, which becomes more pronounced with increasing d. We ascribed such peculiar T and d dependence to the crossover phenomenon from the coupled state to the decoupled one between the top and the bottom electron accumulation layers possessing a large superconducting order parameter Δ_{SC} though the bulky middle region with a small Δ_{SC}. Our findings

that anisotropic superconducting properties of FeSe-EDLT stem from a peculiar distribution of the superconducting order parameter likely provide important knowledge for the device application based on the high-T_c FeSe thin film or EDLT.

[1] T. K. Worthington, W. J. Gallagher, and T. R. Dinger, Phys. Rev. Lett. **59**, 1160 (1987).

[2] G. Blatter, M. V. Feigel'man, V. B. Geshkenbein, A. I. Larkin, and V. M. Vinokur, Rev. Mod. Phys. **66**, 1125 (1994).

[3] J. H. Kang, R. T. Kampwirth, and K. E. Gray, Appl. Phys. Lett. **52**, 2080 (1988).

[4] T. T. M. Palstra, B. Batlogg, L. F. Schneemeyer, R. B. van Dover, and J. V. Waszczak, Phys. Rev. B **38**, 5102(R) (1988).

[5] Y. Iye, T. Tamegai, H. Takeya, and H. Takei, Phys. B (Amsterdam, Neth.) **148**, 224 (1987).

[6] Y. Iye, S. Nakamura, and T. Tamegai, Phys. C (Amsterdam, Neth.) **159**, 433 (1989).

[7] J.-M. Triscone, Ø. Fischer, O. Brunner, L. Antognazza, A. D. Kent, and M. G. Karkut, Phys. Rev. Lett. **64**, 804 (1990).

[8] H. Q. Yuan, J. Singleton, F. F. Balakirev, S. A. Baily, G. F. Chen, J. L. Luo, and N. L. Wang, Nature **457**, 565 (2009).

[9] S. I. Vedeneev, B. A. Piot, D. K. Maude, and A. V. Sadakov, Phys. Rev. B **87**, 134512 (2013).

[10] P. de Trey, S. Gygax, and J.-P. Jan, J. Low Temp. Phys. **11**, 421 (1973).

[11] X. Xi, Z. Wang, W. Zhao, J.-H. Park, K. T. Law, H. Berger, L. Forró, J. Shan, and K. F. Mak, Nat. Phys. **12**, 139 (2016).

[12] Y. Saito, Y. Nakamura, M. S. Bahramy, Y. Kohama, J. Ye, Y. Kasahara, Y. Nakagawa, M. Onga, M. Tokunaga, T. Nojima, Y. Yanase, and Y. Iwasa, Nat. Phys. **12**, 144 (2016).

[13] J. R. Clem, Phys. Rev. B **43**, 7837 (1991).

[14] Y. Matsuda, S. Komiyama, T. Onogi, T. Terashima, K. Shimura, and Y. Bando, Phys. Rev. B **48**, 10498 (1993).

[15] K. Murase, S. Ishida, S. Takaoka, T. Okimura, H. Fujiyasu, A. Ishida, and M. Aoki, Surf. Sci. **170**, 486 (1986).

[16] N. Reyren, S. Gariglio, A. D. Caviglia, D. Jaccard, T. Schneider, and J.-M. Triscone, Appl. Phys. Lett. **94**, 112506 (2009).

[17] M. P. Maley, J. Appl. Phys. **70**, 6189 (1991).

[18] Y. Kamihara, T. Watanabe, M. Hirano, and H. Hosono, J. Am. Chem. Soc. **130**, 3296 (2008).

[19] G. R. Stewart, Rev. Mod. Phys. **83**, 1589 (2011).

[20] H. Hiramatsu, T. Katase, T. Kamiya, and H. Hosono, J. Phys. Soc. Jpn. **81**, 011011 (2012).

[21] F. C. Hsu, J. Y. Luo, K. W. Yeh, T. K. Chen, T. W. Huang, P. M. Wu, Y. C. Lee, Y. L. Huang, Y. Y. Chu, D. C. Yan, and M. K. Wu, Proc. Natl. Acad. Sci. U.S.A. **105**, 14262 (2008).

[22] J. L. Her, Y. Kohama, Y. H. Matsuda, K. Kindo, W. H. Yang, D. A. Chareev, E. S. Mitrofanova, O. S. Volkova, A. N. Vasiliev, and J. Y. Lin, Supercond. Sci. Technol. **28**, 045013 (2015).

[23] Q. Y. Wang, Z. Li, W. H. Zhang, Z. C. Zhang, J. S. Zhang, W. Li, H. Ding, Y. B. Ou, P. Deng, K. Chang, J. Wen, C. L. Song, K. He, J. F. Jia, S. H. Ji, Y. Y. Wang, L. L. Wang, X. Chen, X. C. Ma, and Q. K. Xue, Chin. Phys. Lett. **29**, 037402 (2012).

[24] W. H. Zhang, Y. Sun, J. S. Zhang, F. S. Li, M. H. Guo, Y. F. Zhao, H. M. Zhang, J. P. Peng, Y. Xing, H. C. Wang, T. Fujita, A. Hirata, Z. Li, H. Ding, C. J. Tang, M. Wang, Q. Y. Wang, K. He, S. H. Ji, X. Chen *et al.*, Chin. Phys. Lett. **31**, 017401 (2014).

[25] J. Shiogai, Y. Ito, T. Mitsuhashi, T. Nojima, and A. Tsukazaki, Nat. Phys. **12**, 42 (2016).

[26] J. Shiogai, T. Miyakawa, Y. Ito, T. Nojima, and A. Tsukazaki, Phys. Rev. B **95**, 115101 (2017).

[27] K. Watanabe, S. Awaji, H. Oguro, Y. Tsuchiya, S. Hanai, H. Miyazaki, T. Tosaka, M. Takahashi, and S. Ioka, J. Phys.: Conf. Ser. **568**, 032019 (2014).

[28] S. Awaji, K. Watanabe, H. Oguro, H. Miyazaki, S. Hanai, T. Tosaka, and S. Ioka, Supercond. Sci. Technol. **30**, 065001 (2017).

[29] K. Hanzawa, H. Sato, H. Hiramatsu, T. Kamiya, and H. Hosono, Proc. Natl. Acad. Sci. U.S.A. **113**, 3986 (2016).

[30] B. Lei, J. H. Cui, Z. J. Xiang, C. Shang, N. Z. Wang, G. J. Ye, X. G. Luo, T. Wu, Z. Sun, and X. H. Chen, Phys. Rev. Lett. **116**, 077002 (2016).

[31] H. Iwasaki, O. Taniguchi, S. Kenmochi, and N. Kobayashi, Phys. C (Amsterdam, Neth.) **244**, 71 (1995).

[32] H. Raffy, S. Labdi, O. Laborde, and P. Monceau, Phys. Rev. Lett. **66**, 2515 (1991).

[33] C. M. Fu, V. V. Moshchalkov, W. Boon, K. Temst, Y. Bruynseraede, G. Jakob, T. Hahn, and H. Adrian, Phys. C (Amsterdam, Neth.) **205**, 111 (1993).

[34] Z. R. Ye, C. F. Zhang, H. L. Ning, W. Li, L. Chen, T. Jia, M. Hashimoto, D. H. Lu, Z. X. Shen, and Y. Zhang, arXiv:1512.02526.